Electronic states of the $C_6H_6/Cu\{111\}$ system: Energetics, femtosecond dynamics, and adsorption morphology

Cite as: J. Chem. Phys. **109**, 9155 (1998); https://doi.org/10.1063/1.477468
Submitted: 06 May 1998 . Accepted: 19 August 1998 . Published Online: 13 November 1998

D. Velic, A. Hotzel, M. Wolf, and G. Ertl

Electronic states of the C_6H_6/Cu{111} system: Energetics, femtosecond dynamics, and adsorption morphology

D. Velic, A. Hotzel, M. Wolf,[a] and G. Ertl
Fritz-Haber-Institut der Max-Planck-Gesellschaft, Faradayweg 4-6, D-14195 Berlin, Germany

(Received 6 May 1998; accepted 19 August 1998)

Two-photon-photoemission (2PPE) spectroscopy is employed to characterize electronic states of a bilayer C_6H_6/Cu{111} system at 85 K. The unoccupied benzene π^* e_{2u} state is observed with a binding energy of 4.6 eV above the Fermi level. This result agrees with inverse-photoemission (IPE) data and provides a case where the determination of the binding energy is identical for 2PPE and IPE. The π^* e_{2u} state is assigned in the 2PPE scheme as a final state which is the first observed final state in 2PPE of adsorbate-surface systems. The dependence of the electron dynamics on the morphology of an incomplete adsorption layer is also investigated. Two $(n=1)$-like image potential states *A* and *B* are observed which presumably originate from two different C_6H_6 adsorption geometries in the bilayer regime. The two image states *A* and *B* are characterized by electron effective masses of 1.1 and 1.9 m_e, binding energies of 3.30 and 3.45 eV above the Fermi level, and lifetimes of 40 and 20 fs, respectively. The dielectric continuum model and the Kronig–Penney model are employed to simulate the origin of $(n=1)$-like image states. The work function decreases from 4.9 eV at clean Cu{111} to 4.0 eV at bilayer coverage. The change of the work function and the observation of two image states suggest the redefining of the ratio of the numbers of benzene molecules in the first and the second layers of the bilayer regime to approximately 1:1 instead of 1:2, as previously reported. 2PPE is shown to be sensitive to the changes of morphologies, local work functions, and adsorbate-surface potentials during the layer formation. © *1998 American Institute of Physics.* [S0021-9606(98)70344-7]

I. INTRODUCTION

Electronic excitation is an important step in chemical reactions. The energetics and lifetime of this process directly govern the reaction probability. In order to possibly control a pathway along the reaction coordinate, the electron dynamics must be determined. The time scale of elementary electronic processes varies from pico to femtoseconds, and, only the progress in ultrafast laser technology has allowed the probing of such fast events at surfaces in real time.[1] In recent years, time-resolved two-photon-photoemission (2PPE) spectroscopy has been employed to determine the dynamics of photoexcited electrons with energy and momentum resolution on the femtosecond time scale.[2] 2PPE was used in various adsorbate-surface systems to study adsorbate-induced and image potential states.[2–17] The variety of adsorbates investigated on the Cu{111} surface spans from small molecules, like CO,[7] through atomic overlayers, like Xe,[9] to larger molecules, like C_6H_6.[14,15] In this paper we present a 2PPE investigation of the C_6H_6 bilayer coverage on Cu{111}. This system was chosen for two main reasons. The first reason is to electronically characterize the adsorbed benzene molecule which traditionally serves as a model system for large molecules. The benzene π^* e_{2u} state is observed in the 2PPE spectrum at 4.6 eV above the Fermi level, in agreement with inverse photoemission (IPE).[18] This state is assigned in the 2PPE scheme as the final state which represents the first observation of an adsorbate-induced final state. Previously, Giesen *et al.*[17] observed a similar final state behavior on Ag{111}, which was, however, assigned to energy pooling between two electrons in an intermediate image potential state. The second reason to study the C_6H_6/Cu{111} system is the complex adsorption geometry of the benzene bilayer[19] which is used to investigate the influence of the incomplete layer morphology on electron dynamics. The formation of two $(n=1)$-like image states *A* and *B* is observed, presumably as a result of different adsorption geometries in the first and the second layer of benzene. The femtosecond dynamics of these two states is determined, presenting a first measurement of the electronic lifetimes in an incomplete layer of adsorbates. The 2PPE was shown to be sensitive to local work functions and adsorbate-surface potentials which are associated, in this case, with the different benzene adsorption morphologies. This study can also shed some light on the electron dynamics of inhomogeneous or laterally confined systems.

Lowest unoccupied (LUMO) and highest occupied molecular orbitals (HOMO) of adsorbates are of interest for rehybridization with the bulk bands.[20] Using 2PPE, the lifetime of the CO LUMO on Cu{111} was recently determined to be less than 5 fs.[7] Another class of electronic surface states is formed by the Coulombic tail of the image potential.[8–10] The wave functions of these image potential states are localized at the surface and decay exponentially into the bulk. The lifetimes of image states were previously investigated. In general,[5,9] with an increasing number of physisorbed adsorbate layers, the lifetimes of image states are

[a]Electronic mail: wolf@fhi-berlin.mpg.de; fax: +49 30 84135106.

found to increase, because the wave functions are located farther away from the surface. Interestingly, Hotzel *et al.*[8] showed that the lifetime of a surface state in O_2/Xe/Cu{111} decreases with increasing number of Xe spacer layers, as a result of coupling between the $n=1$ image state and a negative ion resonance of the molecular oxygen $X\ ^2\Pi_g$ state. Another complex behavior of image states was observed for cyclohexane/Ag{111} and *n*-heptane/Ag{111}.[5] The observed multiple peaks of the $n=1$ image state at the cyclohexane bilayer coverage were attributed to the incomplete layer growth. Double peaks of the $n=1$ state were also observed in the Ag/Pd{111} system.[3] In these cases, 2PPE was shown to be sensitive to the growth morphology of adsorbate layers.

The C_6H_6/Cu{111} system was previously studied with 2PPE,[14,15] temperature programmed desorption (TPD), high-resolution electron energy loss spectroscopy (HREELS), near-edge X-ray absorption fine structure (NEXAFS),[19] IPE,[18] and scanning tunneling microscopy (STM).[21] Using 2PPE, Munakata *et al.*[14,15] observed a spectral fine structure of C_6H_6/Cu{111} at about 1 eV above the Fermi level. The state responsible for this structure was assigned as the excited lowest triplet state of adsorbed benzene.[14] Based on the HREELS and NEXAFS results, the estimated benzene coverage, and the size of the C_6H_6 molecule, Xi *et al.*[19] concluded that the benzene molecules in the first and the second layer of the bilayer regime are oriented with their π rings approximately parallel and perpendicular to the surface plane, respectively.[19] The picture of flat-lying benzene at low coverages was also supported by STM measurements[21] as well as by theoretical calculation.[22] The IPE[18] spectrum of C_6H_6/Cu{111} showed the twofold degenerate antibonding e_{2u} state (LUMO) of benzene at 4.6 ± 0.1 eV above the Fermi level with a full width at half maximum (FWHM) of 1.2 ± 0.2 eV.

II. EXPERIMENT

The 2PPE experiments were performed in an ultrahigh vacuum chamber (1×10^{-10} mbar) equipped with a custom designed electron time-of-flight (TOF) spectrometer and coupled to a femtosecond laser system. The details of this experimental setup were described elsewhere.[10] Briefly, a 200 kHz femtosecond Ti-sapphire oscillator/amplifier (Coherent, Mira 900/RegA 9000), pumped with an argon ion laser (Coherent, Innova 400), and pumping an optical parametric amplifier (Coherent, OPA 9400), was used. Tunable visible (VIS) pulses of the OPA at wavelengths between 470 and 730 nm were used to generate ultraviolet (UV) second harmonic pulses in a 0.2 mm thick beta barium borate crystal. The temporal widths of the VIS and UV pulses were compressed by two pairs of prisms to achieve pulse duration of <80 fs. In the time-resolved 2PPE experiments, the UV and VIS pulses were delayed with respect to each other, using a translation stage. The pulses were then noncollinearly ($<0.5°$ skew) focused on the Cu{111} crystal. The temporal spread introduced by this skew angle was estimated to be less than 5 fs.[11] The laser beams, which were either *p*- or *s*-polarized, were incident on the sample under 45° with respect to the surface normal. Photoemitted electrons were detected within $\pm3.5°$ along the surface normal ($k_{\|}=0$) after drifting through the 300 mm field-free region of the TOF spectrometer, which had an energy resolution of 8 meV (FWHM) at 1 eV kinetic energy.[8] In the dispersion measurements the detection angle was varied. To avoid space charge, rise of the electronic temperature, and laser induced modification of the C_6H_6 layers, a low pulse fluence of 10 μJ/cm^2 was used.

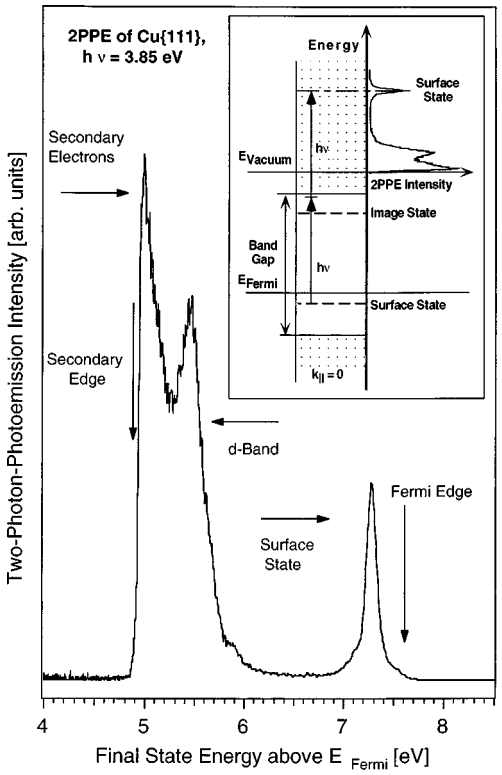

FIG. 1. 2PPE spectrum of Cu{111} at 85 K, plotted as 2PPE intensity vs final state energy above the Fermi level. The inset describes the 2PPE process where two photons are required to emit an electron from the occupied surface state into the vacuum. The left side of the inset represents the Cu{111} bulk, consisting of electronic bands (dotted) and the *sp*-band gap (white) along $k_{\|}=0$, and the right side represents the vacuum. The spectrum in the inset is identical with the main plot.

The Cu{111} crystal was mounted on a manipulator equipped with heating and cooling units. The Cu{111} surface was cleaned by standard sputtering-annealing cycles,[23] and the benzene was purified by a freeze–pump–thaw method prior to dosing. The benzene was dosed through a pinhole doser (5 mm hole, 2 cm away from the surface, 0.5 mbar back-pressure of the doser). The temperatures of the crystal during the dosing and the 2PPE measurements were 120 and 85 K, respectively.

III. RESULTS AND DISCUSSION

A. 2PPE from Cu{111}

The 2PPE spectrum of clean Cu{111} at 85 K is shown in Fig. 1, plotted as 2PPE intensity versus final state energy above the Fermi level. The spectrum shows four main features: a secondary electron peak (the vacuum energy edge), the Cu *d*-band peak, the peak of the Cu{111} surface state, and the Fermi edge. Using the 2PPE spectrum shown in Fig. 1, which was measured with 3.85 eV photon energy, the

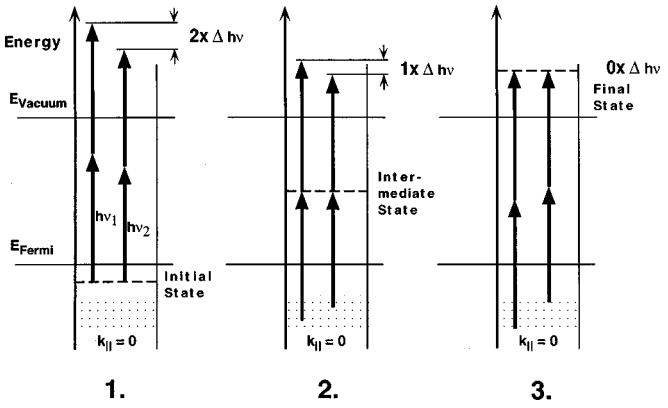

FIG. 2. The variation of a 2PPE peak with the photon energy allows us to distinguish between an initial state peak (1), an intermediate state peak (2), and a final state peak (3). The initial state peak varies with twice the photon energy ($2\times\Delta h\nu$; $\Delta h\nu = h\nu_1 - h\nu_2$), the intermediate state peak with once the photon energy ($1\times\Delta h\nu$), and the final state peak does not vary with the photon energy.

work function is determined to be 4.9 eV. This value of the Cu{111} work function and also the calculated surface state binding energy of 0.4 eV below the Fermi level are in agreement with previously measured values of 4.93[2] and 0.42 eV at 25 K,[11] respectively.

The nature of the 2PPE is shown in the inset of Fig. 1 for 2PPE from the surface state on Cu{111}. The left side of the inset represents the Cu{111} bulk electronic structure, consisting of electronic bands (dotted) and the *sp*-band gap (white) along $k_{\|}=0$, and the right side represents the vacuum. The spectrum shown in the inset is identical to the main plot. With 3.85 eV photon energy, two photons are required to observe the 2PPE surface state peak where the electron is excited from the occupied surface state via a virtual state to the final state above the vacuum level. However, 2PPE probes both occupied and unoccupied states and can also distinguish between the unoccupied intermediate and the unoccupied final states, as discussed below.

The detailed 2PPE schemes in Fig. 2 show how to identify an initial state, Fig. 2-1, an intermediate state, Fig. 2-2, and a final state, Fig. 2-3. The schemes present the wavelength dependence of these states where the 2PPE peak energy varies with the photon energy. To illustrate this dependence, we used two different photon energies, $h\nu_1$ and $h\nu_2$. Figure 2-1 shows that the energy of a photoemitted electron from a discrete occupied initial state below the Fermi level varies with twice the photon energy difference $[2x\Delta h\nu = 2x(h\nu_1 - h\nu_2)]$. Figure 2-2 shows that for a peak arising from an intermediate state, like an image state, the kinetic energy varies with once the photon energy ($1x\Delta h\nu$). Finally, Fig. 2-3 shows that the energy of a final state peak does not vary with the photon energy in 2PPE.

B. Work function of C_6H_6/Cu{111} and definition of ML

The benzene adsorption results in a decrease of the work function which is attributed to an electron-donating character of C_6H_6. As shown in Fig. 3, the work function change was studied as a function of the benzene adsorption coverage.

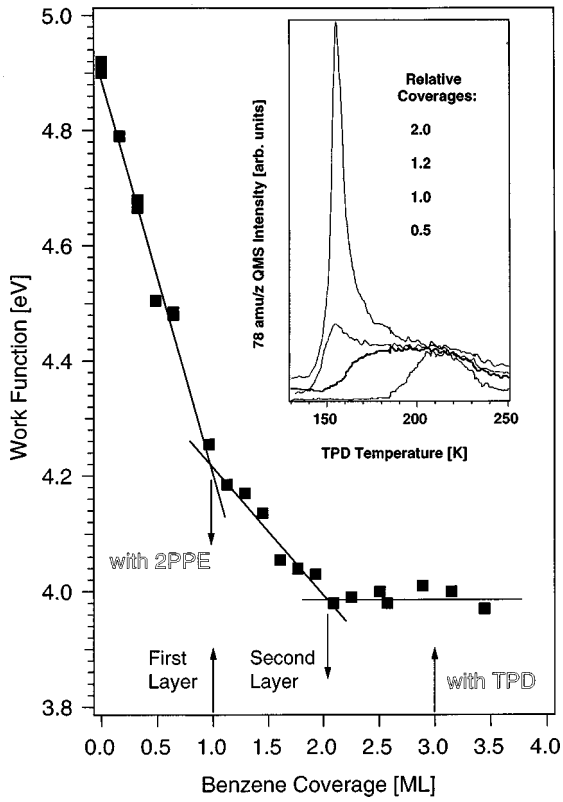

FIG. 3. Work function vs benzene coverage on Cu{111}. Three different linear trends correspond to the formation of the first, the second, and the multilayers, respectively. The upward and downward arrows indicate the assignments of monolayer and bilayer completions based on TPD and 2PPE, respectively. The inset shows the TPD spectra of C_6H_6 from Cu{111} where the 1.0 curve represents the first layer of benzene on Cu{111} and defines the 1 ML coverage.

Before this dependence is discussed, we define a unit of coverage. The inset of Fig. 3 shows the TPD data, as the quadrupole mass spectrometer (QMS) intensity of mass 78 plotted versus the desorption temperature, which are used to define one monolayer (1 ML). The inset shows four desorption curves assigned as 0.5, 1.0, 1.2, and 2.0. These numbers represent the relative integrated TPD intensities in comparison with the intensity of the 1.0 curve. The TPD curve of 1.0 is identical with the TPD measurement by Xi *et al.*,[19] and the corresponding coverage, representing the formation of the first benzene layer on Cu{111}, is defined as 1 ML.

Based on the TPD results,[19] three coverage regimes were observed: (i) the monolayer regime at exposures below 2.5 L ($1\ \mathrm{L}=10^{-6}$ Torr s) where the TPD peak temperature shifted from 240 to approximately 150 K with the benzene exposure, (ii) the bilayer regime observed between 2.5 and 7 L with the TPD peak approximately constant at 155–157 K, and (iii) the multilayer regime at exposures above 7 L where the TPD peak shifted to 152 K. The main reason to also present our TPD measurements here is to clearly define the monolayer as a coverage unit which is used in this paper. Note that because our TPD data and the results presented by Xi. *et al.*[19] are identical, the bilayer and multilayer TPD curves are not shown. The TPD peak temperature is observed to be approximately constant during the bilayer formation with a value of 155 K, which is represented by the 2.0 curve

shown in the inset of Fig. 3. The further change of the TPD peak temperature from 155 to approximately 150 K was proposed to correspond to the multilayer formation. Using TPD and HREELS, Xi *et al.* estimated the ratio of the numbers of benzene molecules in the first and the second layer to be 1:1.8.[19] Based on our TPD measurements, this ratio in the bilayer coverage was estimated to be the same, about 1:2. However, this coverage is contradictory to the density of solid benzene where the ratio of the numbers of benzene molecules in two adjacent layers is 1:1.[24] Using 2PPE results, our arguments to redefine the coverage of the bilayer completion on Cu{111} are discussed in Sec. III D 2.

The main panel of Fig. 3 presents the dependence of the work function on the benzene coverage. The coverages for the 2PPE experiments were obtained from subsequent TPD measurements and expressed in ML, as discussed above. The two downward arrows point out the coverages where the completions of the first and the second layer are observed, based on the work function change. Note that the upward arrows point out the coverages of layer completions, based on the TPD results. The work function dependence on the benzene coverage displays three linear trends: below 1, between 1 and 2, and above 2 ML. The first trend is a decrease from 4.9 for clean Cu{111} to 4.2 eV for 1.0 ML coverage. We note the agreement between the first layer completion assigned by TPD and the work function trend. This agreement is demonstrated in Fig. 3 by the overlap of downward and upward arrows at 1 ML. Zhou *et al.*[25] investigated the similar system of C_6H_6/Ag where the work function change for the first layer was measured to be -0.7 eV. The second trend is a further decrease with a smaller slope from 4.2 to 4.0 eV, due to the second layer formation. The surface is saturated with respect to the change of the work function at approximately 2.0 ML. Interestingly, this trend, further discussed in Sec. III D 2, does not coincide with the completion of the second layer as estimated by TPD. The third trend is a constant work function with increasing coverage during multilayer formation above 2.0 ML.

C. 2PPE of C_6H_6/Cu{111}

1. Coverage dependence

In Fig. 4, two sets of 2PPE spectra measured at two photon energies are displayed. At low coverages of 0.1, 0.3, and 0.5 ML, a photon energy of 4.12 eV was used. The spectrum of 0.1 ML shows the *d*-band peak and the broadened surface state peak. The broadening of the surface state during the initial adsorption of benzene is in agreement with the result of Munakata *et al.*[15] Such a broadening of the surface state might be explained by the interaction of Cu and benzene where the benzene HOMO might be involved. The energy differences between the benzene b_{2g} and e_{2u} (LUMO) states in the gas phase and on Ag{111} are approximately the same.[18] Therefore, we assume that also on Cu{111} the energy differences between the molecular orbitals are approximately the same as in the gas phase. Using the e_{2u} position of C_6H_6[18] and the energy spacing in gas phase benzene,[26] we estimated the binding energy of the benzene HOMO to be approximately 0.5 eV below the Fermi level,

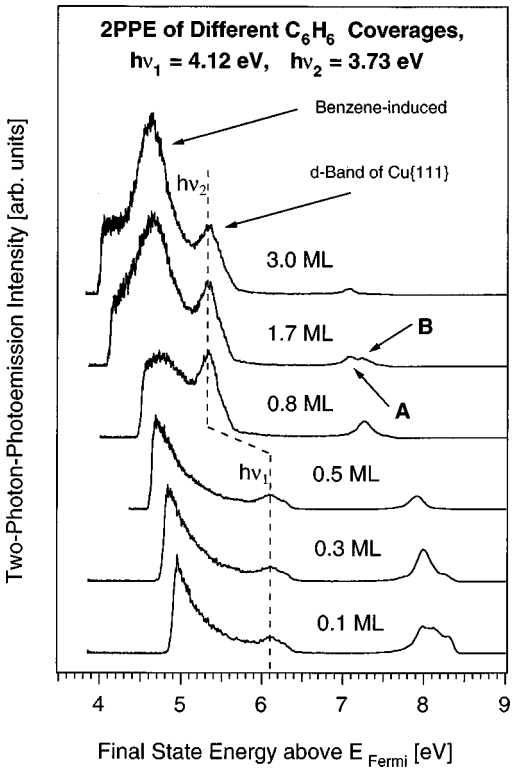

FIG. 4. 2PPE spectra of C_6H_6/Cu{111} measured at two different photon energies. At low coverages the *d*- band peak and the broadened surface state peak are observed. At the benzene coverage of approximately 1.7 ML, a benzene-induced peak appears close to the secondary edge, the *d*-band peak of Cu{111} remains qualitatively unchanged, and the surface state peak progresses into two peaks A and B.

close to the surface state. The spectral broadening of the surface state might thus indeed be attributed to an interaction between the surface state and the benzene HOMO. However, this interaction is not discussed in this paper, as the main focus is on the bilayer regime. At higher coverages of 0.8, 1.7, and 3.0 ML, as shown in Fig. 4, a photon energy of 3.73 eV was used to avoid one-photon photoemission. At the benzene coverage of approximately 1.7 ML, a new benzene-induced peak appears close to the secondary edge, the *d*-band peak of Cu{111} remains qualitatively unchanged, only shifted due to the different photon energy, and the surface state peak develops into two peaks which are labeled as states *A* and *B* with increasing kinetic energy. The progression and characterization of the peaks A and B are discussed in Sec. D.

The low coverage regime is of interest, because Munakata *et al.*[14,15] observed the fine structure of C_6H_6/Cu{111} at the exposure of 0.32 L. Their spectrum, measured with 3.87 eV photon energy, showed a progression of four peaks of less than 0.2 width, with about 0.2 eV spacing. These features were proposed to originate from benzene-induced excited states about 1 eV above the Fermi level. Using the exposure of 0.32 L and Munakata's reported factor of 2^{14} between his and Xi's exposures,[19] the corresponding coverage is estimated to be 0.4 ML. However, Fig. 4 shows no fine structure at this coverage. This submonolayer coverage should induce a work function change of approximately -0.3 eV, based on the results shown in Fig. 3. However, this

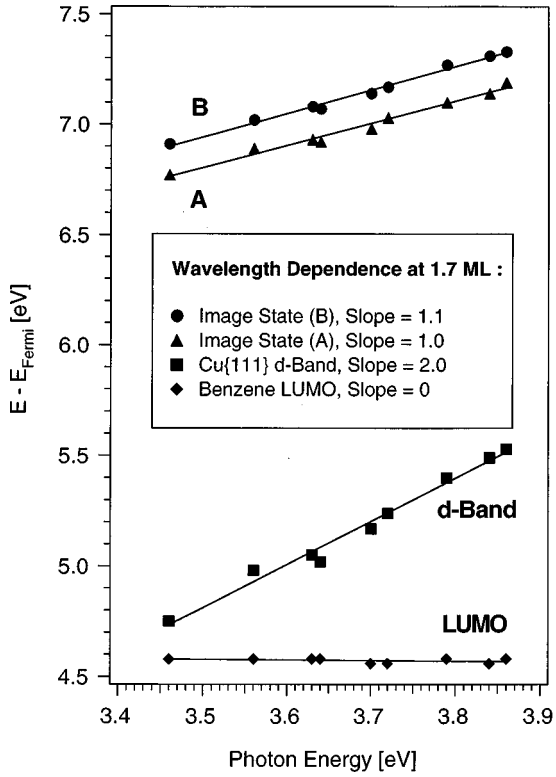

FIG. 5. The wavelength dependence of the C_6H_6/Cu{111} 2PPE peak positions. The energy above the Fermi level is plotted vs the laser photon energy. At the benzene coverage of 1.7 ML, all four features are observed: the benzene-induced peak (rhombs) assigned as the C_6H_6 LUMO, the Cu *d*-band peak (squares), and the A (triangles) and B (circles) peaks assigned as image states.

is not the result presented by Munakata *et al.*,[14] where the work function change was estimated to be about -0.8 eV. At the higher coverage of 1.7 ML, as shown in Fig. 4, the work function change is -0.8 eV. Using the comparable photon energy as Munakata *et al.*, only one broad peak is observed in the energy range from 4 to 5 eV above the Fermi level where Munakata *et al.* observed the fine structure.[14] Concluding, we report that the fine structure is not reproduced in our experiments at any coverage. A possible explanation could be that these features are a result of either some spatial or temporal inhomogeneities of the benzene coverage. Note that Stranick *et al.* observed with STM a formation of benzene islands which diffuse freely at 77 K on Cu{111} at submonolayer coverage.[21]

2. Wavelength dependence

In order to characterize the 2PPE features of C_6H_6/Cu{111}, the wavelength dependence of the peak positions is analyzed, as shown in Fig. 5. The photon energy was tuned from 3.46 to 3.87 eV for a benzene coverage of 1.7 ML where all the features are observed: the benzene-induced peak near the secondary edge (rhombs), the Cu *d*-band peak (squares), and the A (triangles) and B (circles) peaks. The four data sets show linear dependences on the photon energy and their fits yield slopes of 0, 2.0, 1.0, and 1.1, respectively. Note that the detailed schemes of the 2PPE process are displayed in Fig. 2. All the 2PPE spectra presented in this paper are measured with *p*-polarized light (electric field vector parallel to the plane of incidence). Using *s*-polarized light, the benzene-induced peak near the secondary edge and the Cu *d*-band peaks remain unchanged, but the peaks A and B disappear, suggesting that the states *A* and *B* have σ-symmetry.

The benzene-induced peak near the secondary edge shows no kinetic energy dependence on photon energy (slope$=0$) and can be assigned as a final state in the 2PPE scheme, as illustrated in Fig. 2-3. The binding energy of this state is calculated to be 4.6 ± 0.05 eV above the Fermi level with a FWHM of 0.5 eV. In accordance with the IPE[18] result determining the benzene LUMO π^* e_{2u} state at 4.6 eV above the Fermi level, we assign the 2PPE benzene-induced peak as the LUMO state. The polarization dependence of the benzene-induced peak is also consistent with e_{2u} symmetry. The observation of this adsorbate-induced final state is somehow unique in 2PPE investigations reported so far.

Traditionally, unoccupied electronic states are determined by IPE. 2PPE then represents an alternative technique to probe these states. The comparison of the binding energies determined by these two techniques is of interest, because of their different excitation mechanisms. In principle, the binding energies measured with IPE and 2PPE could differ, because their final states are systems with $(n+1)$ and $(n-1)$ electrons, respectively. In the case of IPE, an electron is added to the system and a photon is detected. In the case of 2PPE, a photon is used to emit an electron from the system. The agreement between the determined binding energies suggests that the 2PPE photohole is generated in the Cu bulk, allowing the complete screening of the hole on the time scale of the 2PPE process. Interestingly, the results of x-ray emission and absorption of C_6H_6/Cu{110}[27] do not provide a similar binding energy for the π^* e_{2u} state. In this case, the photohole is located at the carbon atom and presumably cannot be effectively screened on the time scale of the absorption/emission processes. We conclude that our 2PPE result describes an experimental case where the photohole is screened and therefore, the binding energies determined by 2PPE and IPE are in agreement.

The C_6H_6 coverage used in the IPE measurement[18] was estimated to be (2 ± 1) monolayers. However, it was not discussed whether the observed LUMO at 4.6 eV above the Fermi level was the e_{2u} state of the molecules in the first or in the second layer. In general, the energetic position of an unoccupied molecular orbital is lower in a molecule adsorbed on a metal surface than in a free molecule. Three effects contribute to this downshift: (i) the image charge screening by the metal substrate, (ii) the polarization of the neighboring adsorbed molecules, and (iii) possible delocalization (band formation) within the adsorbate layers. The e_{2u} state of the C_6H_6 molecule in the gas phase is situated 1.15 eV above the vacuum level.[28] If we for the moment neglect the influence of the neighboring C_6H_6 molecules, the downshift induced by the image charge screening of the metal is given by $-\mathrm{Ry}/(2z)$, where Ry is the Rydberg constant, and z the distance of the molecule from the image plane in units of the Bohr radius. Identifying the image plane with the

metal surface, and assuming a work function of 4.1 eV, the measured LUMO energy is reduced by 0.65 eV compared to the free molecule, which corresponds to a distance of 5.5 Å from the surface. Considering that the first layer consists of flat-lying C_6H_6 molecules,[19] this value is only consistent with the assumption that the measured LUMO is the e_{2u} state of the molecules in the second layer. The e_{2u} state of benzene in the first layer is certainly shifted further down, most probably below the vacuum level. A possible reason why it is not observed in 2PPE might be that it is extremely broadened by the interaction with the metal surface. We can rule out that either state *A* or *B* is the e_{2u} state of the first layer, since these states show σ-symmetry, and the intensities and widths of the peaks are much smaller than those of the observed LUMO of the second layer. In summary, we conclude that the observed e_{2u} state originates from benzene in the second layer.

The position of the Cu *d*-band peak shifts with twice the photon energy (slope=2.0). Such a shift is expected for the occupied initial states, as shown in Fig. 2-1. Both the peak A and the peak B shift with once the photon energy (slope =1.0 and slope=1.1, respectively), a behavior which is expected for intermediate states, as shown in Fig. 2-2. This observation provides the evidence that the *A* and *B* states are unoccupied electronic states with binding energies of 3.30 $\pm$0.10 and 3.45$\pm$0.10 eV above the Fermi level, respectively. The possibility that one of these states could be either an occupied surface state or the benzene HOMO can be ruled out. The polarization dependence showed the σ-symmetry of the states *A* and *B*. Note that the image states were previously shown to have σ-symmetry.[2] Thus, based on their binding energies close to the vacuum level and their σ-symmetry, the states *A* and *B* are assigned as image potential states. The difference between the binding energies of the $n=1$ and $n=2$ image states is typically about 0.5, e.g., 0.57 for clean Cu{111} and 0.48 eV for one monolayer Xe/Cu{111}.[9] The two peaks A and B are spectrally resolved with FWHMs of 0.15 and a peak-to-peak separation of 0.15 eV. Therefore, an assignment of the states *A* and *B* as the $n=1$ and $n=2$ image states, respectively, is unlikely. The absence of the third peak from the $n=3$ state at higher energies also suggests that the peaks A and B are more likely two ($n=1$)-like image states. A detailed discussion of the formation and characterization of the image states *A* and *B* is provided in the following section.

D. Image potential states of C_6H_6/Cu{111}

1. Coverage dependence

The 2PPE peak of the $n=0$ surface state is initially broadened at low benzene coverages and is presumably quenched when the benzene coverage is further increased (see Ref. 18). On the other hand, image potential states have been observed for a wide variety of adsorbate-surface systems at different coverages.[2–17] The evolution of the two image state peaks A and B with benzene coverage is presented in Fig. 6, using 3.65 eV photon energy. The 2PPE intensity is plotted as a function of the binding energy below the vacuum level. The transformation is shown for 2PPE

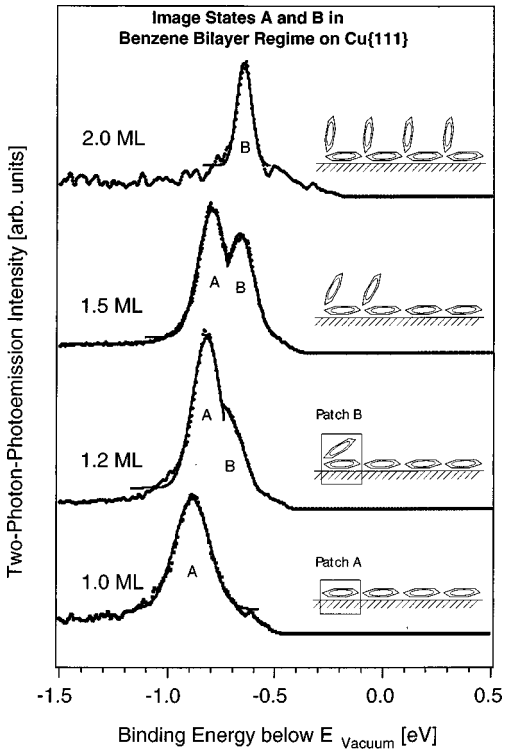

FIG. 6. The evolution of the two image state peaks A and B with the benzene coverage, using 3.65 eV photon energy. The 2PPE intensity is plotted vs the binding energy below the vacuum level. The formation of the two image states is proposed to be induced by the change of the benzene adsorption geometry from the flat-lying benzene molecules in the first layer to the almost vertical benzene molecules in the second layer. The adsorption mechanism is sketched in the four insets where the patch A and the patch B are proposed to provide the different work functions and adsorbate-surface potentials to support the formation of the image states *A* and *B*, respectively.

spectra at benzene coverages of 1.0, 1.2, 1.5, and 2.0 ML. The 2PPE intensities in Fig. 6 are normalized to the *d*- band intensity and the peaks are fitted with Gaussian profiles to guide the eye. Note that the benzene coverage of 1.0 ML corresponds to the completion of the first layer on Cu{111}. Therefore, the 2PPE feature at the 1.0 ML coverage is attributed to a state induced by the first layer of benzene and assigned as the image state *A*. When the benzene coverage is increased above the first layer (1 ML), a shoulder appears on the higher energy side of the image state peak A. The shoulder is attributed to the image state *B* which is presumably induced by the formation of the second layer. At the benzene coverage of 1.5 ML, the two peaks of the image states *A* and *B* are spectrally resolved. Note that because the FWHM of the image state peak A at 1.0 ML coverage is slightly greater than at 1.5 ML, a possible disorder of the first layer cannot be excluded. When the benzene coverage is further increased to 2.0 ML, only one feature is observed and assigned as the image state *B*.

We note that the spectra shown in Fig. 6 were obtained by exposing the crystal to well-defined benzene doses at 120 K. With a different preparation technique, where the crystal was exposed to higher doses and subsequently annealed, a broadened peak with a shoulder was obtained rather than two

well-separated peaks. This behavior might be assigned to differences in the growth morphology.[19]

A similar formation of multiple image state peaks in incomplete adsorbate layers was also observed for the cyclohexane/Ag{111}[5] and Ag/Pd{111}[3] systems. The multiple peaks induced by cyclohexane provided evidence of incomplete layer growth; upon annealing they developed into a single peak. In the case of Ag deposition on Pd{111}, the double peaks were observed in the incomplete layer and only one image state was observed for a complete layer. In this paper the investigation of the image state dynamics is focused on the image states at the intermediate coverage, between the monolayer and the bilayer.

2. Morphology model

The dependence of the *A* and *B* formation on the benzene coverage, shown in Fig. 6, and the correlation between the benzene coverage and the benzene adsorption geometry[19] suggest the following hypothesis. The formation of the two image states is proposed to be induced by two different adsorption morphologies of benzene, progressing from the flat-lying benzene molecules in the first layer to the almost vertical-lying benzene molecules in the second layer. The adsorption scenario is sketched in the four insets of Fig. 6. The change of the work function between the benzene coverages of 1.0 and 2.0 ML was determined to be -0.2 eV. The formation of the two image states is then associated with the work function change and presumably also with a change of the adsorbate-surface potential. In other words, each image state is supported by a different local work function and a different local potential.[3,29] The image state *A* is proposed to be induced by the first layer of flat-lying benzene molecules on the surface. We can visualize a unit which generates the work function change and the adsorbate-surface potential supporting the image state *A*. This ''morphology unit'' is shown in the inset of Fig. 6 by the 1.0 ML peak and assigned as a patch A. When the coverage is increased, the benzene molecules start forming the second layer where they are tilted, as schematically shown in the following insets of Fig. 6. Such a geometry, which is assigned as a patch B, can provide a different work function as well as a different adsorbate-surface potential in comparison with the patch A. The patch B is visualized in the inset of Fig. 6 by the 1.2 ML peak and is proposed to support the formation of the image state *B*.

The experimentally observed coexistence of the two image states, together with the proposed mechanism of the two patches A and B, still leaves open the question of the size of the patches, i.e., whether the benzene molecules of the second layer form islands or are randomly distributed. In the latter case, the state B would be supported by single benzene molecules at coverages slightly above 1 ML, which would imply a localized state with zero dispersion (i.e., infinite effective mass). At coverages close to the bilayer completion, the situation would be reversed, the state *A* would be supported by isolated vacancies, and again show zero dispersion. At intermediate coverage, the states would either remain at zero dispersion, or show an energetic downshift due to delocalization energy. However, as discussed in the following section, the states *A* and *B* show effective masses of 1.1 and $1.9\,m_e$, respectively, at 1.5 ML coverage (m_e = free electron mass), and almost no coverage dependence of their binding energies (Fig. 6). This shows that the patches B which support the respective image state cannot be formed by randomly distributed molecules. We therefore conclude that the incomplete second benzene layer forms islands, and that the image states *A* and *B* are supported by the area between the bilayer islands (patches A), and by the islands themselves (patches B), respectively. In other words, the patches A are identified with the monolayer, and the patches B with the bilayer. This conclusion is supported by the STM observation of freely diffusing benzene islands at submonolayer coverage at 77 K.[21] This result suggests that also the molecules of the second layer, which are more weakly bound according to TPD, can diffuse freely at our experimental conditions, which is prerequisite to island formation.

At 2.0 ML coverage, where the ratio between the numbers of benzene molecules in the first and the second layer is 1:1, only the peak of the image state *B* is observed. The inset of Fig. 6 by the 2.0 ML peak illustrates the saturation of the patches B on the Cu{111} surface. According to TPD, as shown in the inset of Fig. 3, and also according to Xi's results,[19] the complete bilayer is formed at 3 ML coverage where the ratio of the benzene molecules in the first and the second layer is 1:2. Thus, a further growth of the islands and a further decrease of the work function might be expected at coverages above 2.0 ML. However, Fig. 3 shows that the work function is saturated at about 2.0 ML. This result, as well as the observation of the single image state peak B, suggests that the benzene bilayer on Cu{111} is actually completed at 2.0 ML coverage. This conclusion is supported by the structure of solid benzene,[24] where the ratio between the numbers of benzene molecules in two adjacent layers is also 1:1. Therefore, we propose that the ratio between the numbers of benzene molecules in the first and the second layer of the bilayer is approximately 1:1. In this case, the observation of the two image states in 2PPE seems to be more sensitive than TPD in the determination of the benzene bilayer completion. The fact that the FWHM of the image state peak B at 2.0 ML coverage is slightly smaller than at 1.5 ML suggests a more ordered structure at 2.0 ML. This suggestion supports the island-like morphology at 1.5 ML which is more disordered in comparison with the more homogeneous morphology at 2.0 ML. The mechanism presented by a cartoon of the four insets in Fig. 6 qualitatively describes the formation of the two image states. However, the 2PPE intensity ratios of the two image states are not completely explained. This is presumably due to the signal normalization with respect to the Cu *d*-band intensity where the variation of the 2PPE intensity with the coverage is not known.

3. Dispersions of the two image states

The spectrally separated image states *A* and *B* at 1.5 ML coverage, as shown in Fig. 6, are used in the measurements of dispersions and lifetimes. To determine the $k_{\parallel}$ dispersion, the angle between the Cu{111} surface normal and the TOF spectrometer is varied. In these measurements, the bias of the

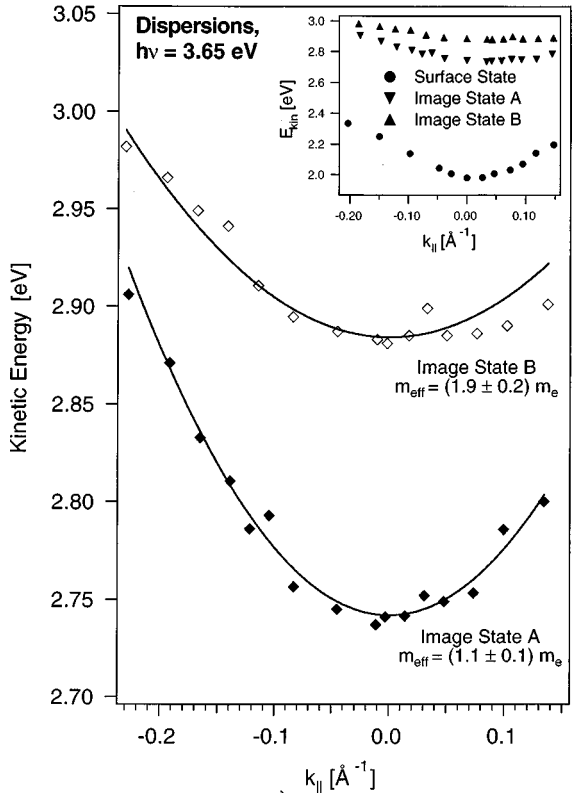

FIG. 7. The dispersion of the image states *A* and *B* parallel to the surface. The parabolic fits (lines) determine the electron effective masses (m_{eff}) with respect to the free electron mass (m_e). The dispersions of the image states *A* and *B* of C_6H_6/Cu{111}, and of the surface state of Cu{111} are compared in the inset.

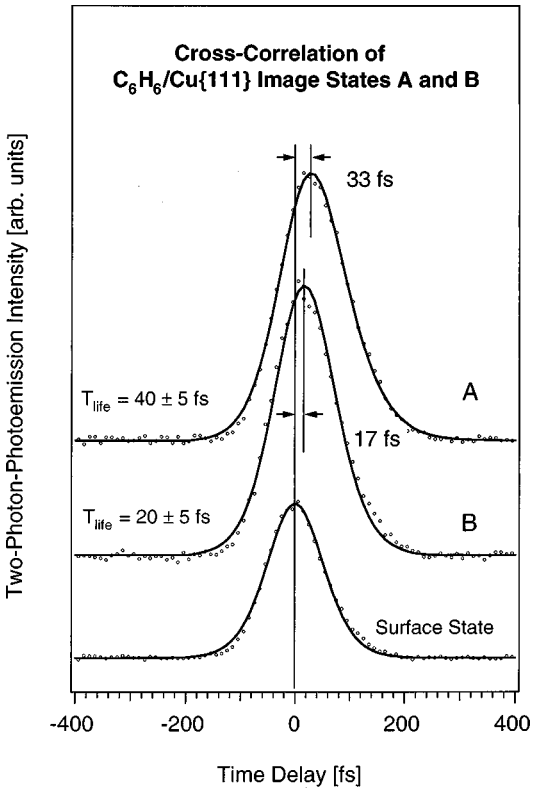

FIG. 8. Cross-correlation curves (data points) of the image states *A* and *B*. The photon energies of 1.88 and 3.75 eV were used at 1.5 ML C_6H_6 coverage. The cross correlation of the Cu surface state is the measure of the temporal shapes of the laser pulses. The fits (lines) of the cross-correlation curves of the image states *A* and *B* yield the lifetimes, which are approximately proportional to the shifts of the maxima of the curves with respect to time zero.

crystal is adjusted to match the vacuum energies between Cu{111} and the TOF spectrometer (graphite coated with a work function of about 4.5 eV). This adjustment minimizes the deviation of electrons due to the external electric field, before they enter the field-free region inside the spectrometer. The beam position on the sample is optimized for the maximum 2PPE signal intensity with a gate on an image state peak. The measured kinetic energy of the photoelectrons (E_k), the angle with respect to the surface normal (θ), and the free electron mass (m_e) are used to calculate the $k_\parallel$ component of the electron wave vector,[5]

$$k_\parallel = (2m_e E_k/\hbar^2)^{1/2} \sin\ \theta. \tag{1}$$

Figure 7 shows the dependence between the electron kinetic energy and $k_\parallel$ for the image states *A* and *B*. The dispersion measurements are performed with 3.65 eV photon energy. The inset of Fig. 7 compares the dispersions of the C_6H_6/Cu{111} image states *A* and *B* and the Cu{111} surface state. The dispersion curves of the image states *A* and *B* were fitted by a parabolic[5] function,

$$E_k = E_0 + \hbar^2 k_\parallel^2/(2m_{\text{eff}}). \tag{2}$$

The fits determine the electron effective masses (m_{eff}) for the image states *A* and *B* to be (1.1 ± 0.1) and (1.9 ± 0.2) m_e, respectively. The mass of the image state *A* is almost the free electron mass, suggesting that the potential of the monolayer C_6H_6/Cu{111} is almost flat in the direction parallel to the surface. The higher effective mass of the image state *B* might then be explained with a modulation of the bilayer C_6H_6/Cu{111} potential parallel to the surface, as discussed in Sec. III D 6. This modulation along the patches B may be attributed to the different, almost perpendicular, binding geometry of the benzene molecules in the second layer.

4. Lifetimes of the two image states

In time-resolved 2PPE, the electron temporal evolution can be followed by recording ''snapshots'' of the 2PPE signal intensity as a function of the pump/probe time delay.[9] In order to determine the lifetimes of the image states *A* and *B*, a cross-correlation curve of the surface state on the clean Cu{111] surface is initially recorded as a measure of the temporal shape of the laser pulses. 2PPE from the surface state is an instantaneous process via a virtual state due to the absence of electronic states in the *sp*-band gap of Cu{111}. Therefore, the cross-correlation signal from this state represents the correlation function of the pump/probe laser pulses. The photon energies used in these experiments were 1.88 of VIS and 3.75 eV of UV. The VIS-UV cross-correlation curve for the surface state peak is shown in Fig. 8. This curve is fitted by the convolution of a sech^2 function with itself,[9] assuming that both laser pulses have sech^2 shapes and the same widths. Compared to Gaussian, Lorentzian, and Voigt pulse shapes, the sech^2 shape provides the best fit to the measured cross-correlation pulse profiles.[9] The determined

FWHM of the laser pulses is 80 fs, which is 65% of the FWHM of the measured cross-correlation curve, as shown in Fig. 8. The position of this curve serves as the time zero of the pump/probe delay. Wolf and co-workers showed that the lifetimes of excited states, which are considerably shorter than the laser pulse duration, can be resolved if the precise time zero of the delay is known.[9,10] Figure 8 also shows the cross-correlation curves of the image states *A* and *B*, both fitted with the convolution of two sech^2 functions and an exponential decay function.[9] The maximum of the curve of the image state *A* is shifted by 33 fs with respect to time zero. This positive time delay corresponds to the case where the UV pump pulse arrives before the VIS probe pulse. Comparing the temporal responses between the virtual state and the image state, the observed shift is a consequence of the excitation process and is proportional to the lifetime. The lifetime of the image state *A* obtained from the analysis[9] of the cross-correlation curve is (40 ± 5) fs. The temporal shift and lifetime of the image state *B* are determined to be 17 and (20 ± 5) fs, respectively.

Since the dominant decay channel of image states is electron–electron scattering in the metal substrate, their lifetimes are approximately inversely proportional to their overlaps with the substrate, i.e., the integrated probability densities inside the crystal. On Cu{111}, this overlap depends strongly on the energetic position of the image state. The farther the image state is located from the center of the *sp*-band gap (1.6 eV above the Fermi level) toward the upper band gap edge (4.1 eV above the Fermi level), the shorter its lifetime, due to the longer penetration length of the wave function into the substrate.[9] The image states *A* and *B* with their binding energies of 3.30 and 3.45 are 0.80 and 0.65 eV below the upper band gap edge, respectively. These positions suggest short lifetimes. The lifetimes of the image states *A* and *B* were experimentally determined to be very short, 40 and 20 fs, respectively, but they are clearly different. However, this difference in the lifetimes cannot be explained by the small difference in binding energies of only 0.15 eV. Another possible explanation for the difference could be that defects can enhance the relaxation processes, and therefore decrease the lifetimes. In the case of the image state *B*, the island-like morphology or irregular growth of the second layer in the patches B could lead to scattering of the electrons away from $k_{\|}=0$ to higher $k_{\|}$ values where the Cu *sp*-band gap is smaller, which would lead to a faster decay compared to image state *A*.

5. Simulation using the dielectric continuum model

In the case of Xe multilayers physisorbed on noble metal surfaces, the dielectric continuum model has been successfully employed to simulate the spectroscopic and dynamic properties of image potential states.[6,8,30] In this model, the adsorbate overlayers are treated as a homogeneous dielectric slab whose effect on the image potential is determined by two parameters: the dielectric constant ε and the electron affinity EA. The dielectric constant ε leads to a screening of the image charge in the metal, and to the creation of an additional image potential well at the dielectric–vacuum interface, due to the polarization of the dielectric. The electron affinity EA leads to a constant energy shift of the image potential inside the dielectric slab.

The binding energies of the image states are calculated by solving Schrödinger's equation for the modified image potential in the dielectric slab and on the vacuum side, and matching the wave function to the solutions of the nearly free electron model in the metal substrate. The lifetimes of the image states can also be estimated within this model, since they are approximately inversely proportional to the overlap of the wave function square with the substrate. More details of this model can be found in Refs. 6 and 8.

We have applied the dielectric continuum model to the systems of a monolayer and a bilayer of benzene on Cu{111}, in order to try to reproduce the properties of the image states *A* and *B*. The parameters used were $\varepsilon=2.284$ (liquid benzene[31]) and $\mathrm{EA}=-1.15$ eV (free C_6H_6 molecule[28]). Note that the measured position of the LUMO at 4.6 eV above the Fermi level agrees well with the electron affinity of the free molecule, if we assume that we measured the LUMO of the second C_6H_6 layer (Sec. III C 2). From the bond lengths of C_6H_6, we estimated the thickness of the (flat-lying) C_6H_6 monolayer (patch A) to be 2 Å, and the thickness of the bilayer (patch B) to be 7 Å. The work functions used in the simulation were 4.2 and 4.0 eV for states *A* and *B*, respectively. In order to avoid singularities at the dielectric–vacuum interface, the potentials were linearly interpolated over a range of 2 Å around the interface.

Figure 9 shows the model potentials and the calculated wave function squares of the lowest-lying image states for one and two C_6H_6 layers on Cu{111}, which correspond to the image states *A* and *B*, respectively. The calculated binding energies are 3.41 and 3.52 eV above the Fermi level for the monolayer and the bilayer, which agrees reasonably well with the measured values of (3.30 ± 0.10) and (3.45 ± 0.10) eV, respectively. On the other hand, the calculated overlaps of the wave function squares with the substrate were only 2.4% for the monolayer and $4.0*10^{-3}$% for the bilayer, whereas the measured lifetimes of 40 and 20 fs correspond to overlaps around 10%–20%.[10,32] Thus, the calculated overlap for the image state *B* on the C_6H_6 bilayer is too small by several orders of magnitude. The reason for the small overlap in the simulation can be seen in Fig. 9, where due to the negative electron affinity, the C_6H_6 bilayer acts as a barrier which effectively decouples the image states from the substrate.

A possible explanation for this discrepancy between our model and the experimental findings is that the electron affinity of the C_6H_6 bilayer is actually less negative, so that there is a higher probability density of the image state *B* inside the second C_6H_6 layer. However, since we measured the binding energy of the LUMO to be 4.6 eV above the Fermi level, there is little room for the assumption of a less negative electron affinity of the C_6H_6 molecules in the second layer. An appealing way out of this dilemma lies in the consideration of the structure of the second layer. Since the molecular density is presumed to be the same as in the first layer (Sec. III D 2), while the molecules are oriented more perpendicular to the surface, there is obviously considerable

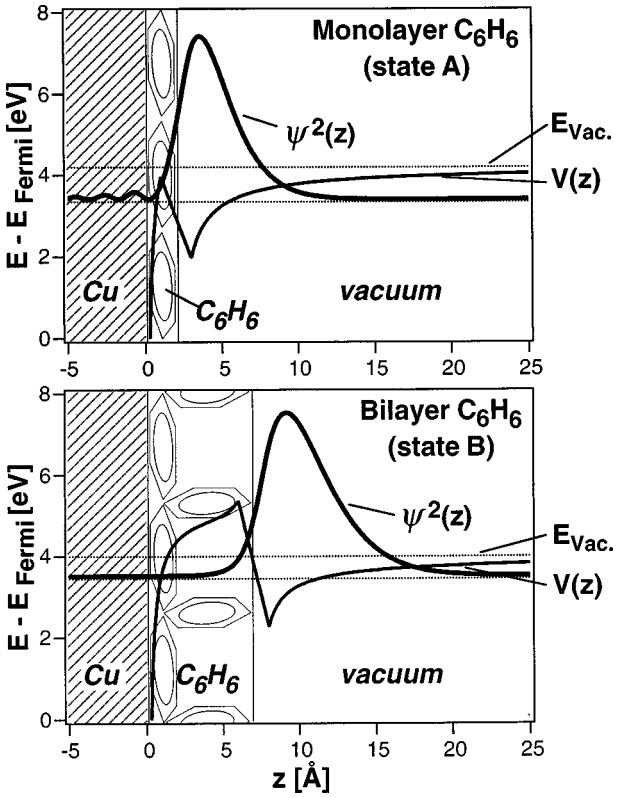

FIG. 9. Simulation of the image states *A* and *B* within the dielectric continuum model. The *z* axis is the direction normal to the surface. The model potentials $V(z)$ are image potentials modified by the presence of the C_6H_6 mono- or bilayer, respectively (indicated by the sketched C_6H_6 molecules). The overlaps of the calculated wave function squares $\psi^2(z)$ with the Cu substrate are approximately inversely proportional to the lifetimes of the states.

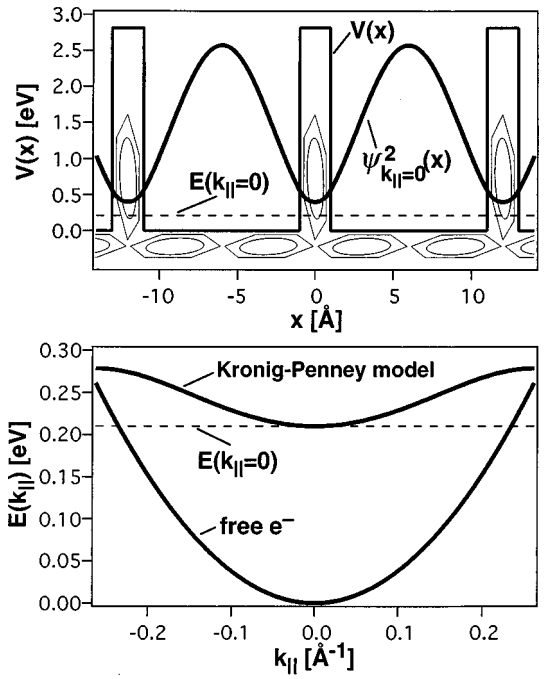

FIG. 10. Kronig–Penney model of the potential parallel to the surface in the second C_6H_6 layer. Upper panel: The model potential $V(x)$ corresponds to a simplified bilayer structure indicated by the sketched C_6H_6 molecules (see text). The calculated wave function square $\psi^2(x)$ for $k_{\|}=0$ is mainly located in the potential wells between the upright molecules of the second layer. The dashed line is the zero line of ψ^2 and indicates the calculated binding energy $E(k_{\|}=0)=0.21$ eV. Lower panel: The calculated dispersion curve for the model potential $V(x)$. The effective mass is 1.9 m_e. The free-electron dispersion curve is shown for comparison.

space between the molecules. If the wave function of the image state *B* is predominantly located between the molecules in the second layer, the effective electron affinity will be something between zero and the electron affinity of the molecules. At the same time, in the direction parallel to the surface, the molecules will act as barriers which reduce the interaction between adjacent potential wells. This will lead to a higher effective mass in the direction parallel to the surface, a prediction which agrees with the experimental finding that the effective mass of image state *B* is 1.9, compared to 1.1 m_e for image state *A*. Thus, both the lifetime and the effective mass of the image state *B* suggest that a considerable part of its wave function is located between the C_6H_6 molecules of the second layer.

6. Kronig–Penney model for the image state B

The relatively loose arrangement of benzene molecules in the second layer leads to a periodic modulation of the electron affinity (and thus of the potential acting on an electron) parallel to the surface (see Fig. 10). This is presumably the reason for the effective mass of 1.9 m_e of the image state *B*. It is suggestive to estimate the effect of this periodic modulation with the aid of the well-known Kronig–Penney model.[33] This model describes the formation of electronic bands in a crystal by a one-dimensional periodic square-well potential.

We have simulated the potential parallel to the surface in the second C_6H_6 layer by a Kronig–Penney potential consisting of periodic square wells (zero potential) of 10 Å width, separated by square barriers (potential U_0) of 2 Å width. These widths correspond roughly to one upright C_6H_6 molecule of the second layer every two flat-lying C_6H_6 molecules of the first layer (see Fig. 10). Assuming that the C_6H_6 bilayer is symmetric in the two dimensions parallel to the surface, this would result in the same number of C_6H_6 molecules in the first and the second layers. Note that the actual structure of the bilayer certainly differs from this simplified model. In order to obtain an effective mass of 1.9 m_e, the barrier height U_0 must be chosen as 2.81 eV, which is considerably higher than the negative electron affinity of 1.15 eV of a single C_6H_6 molecule. However, this difference can be rationalized by the argument that the image state wave function at the position of a C_6H_6 molecule could be a combination of several molecular orbitals, not only the LUMO.

The upper panel of Fig. 10 shows the Kronig–Penney potential used to simulate the potential parallel to the surface in the second C_6H_6 layer, together with the square of the calculated wave function with $k_{\|}=0$. The calculated energy of this state is 0.21 eV. As can be seen in Fig. 10, this energy is mainly the localization energy needed to confine the wave function to the potential wells between the molecules. Considering that the same localization energy will be needed in the other dimension parallel to the surface, this model yields an effective electron affinity of ≈ -0.4 eV, which is indeed

considerably less negative than the value of -1.15 eV of a single C_6H_6 molecule. The lower panel of Fig. 10 shows the dispersion curve parallel to the surface calculated with the Kronig–Penney model potential shown in the upper panel. The curvature at $k_{\|}=0$ corresponds to an effective mass of $1.9\,m_e$. The free-electron dispersion curve is also plotted for comparison.

Concluding, we have shown that a Kronig–Penney model potential with physically meaningful parameters can reproduce the effective mass of $1.9\,m_e$ parallel to the surface observed for the image state *B*. The calculated wave function is mainly localized in the potential wells between the upright C_6H_6 molecules of the second layer, which was postulated in the last section to explain the short lifetime of (20 ± 5) fs of the image state *B*. Thereby, the effective electron affinity of the second C_6H_6 layer is considerably increased compared to the value of -1.15 eV for a single molecule.

IV. CONCLUSION

Two-photon-photoemission spectroscopy was employed to determine the electron dynamics of $C_6H_6/Cu\{111\}$ in the bilayer coverage regime. The C_6H_6 π^* e_{2u} unoccupied state (LUMO) was observed at the binding energy of 4.6 eV above the Fermi level. The LUMO state appeared in the 2PPE scheme as a final state which is the first observed final state in 2PPE for adsorbate-surface systems. An agreement between the binding energies determined with 2PPE and IPE[18] was found, presumably due to effective screening of the photohole. An estimation of the image charge screening suggested that the observed LUMO was the e_{2u} state of the benzene in the second layer.

The work function change was -0.9 eV upon the bilayer formation. Interestingly, 2PPE suggested that the ratio of the numbers of benzene molecules in the first and the second layer is approximately 1:1 instead of 1:2, as previously estimated by TPD and HREELS.[19] Our result is consistent with the structure of solid benzene.

Two image potential states assigned as *A* and *B* were observed at a coverage of approximately 1.5 ML, which is the intermediate benzene coverage between the first and second layers. The binding energies of the image states *A* and *B* were measured to be 3.30 and 3.45 eV above the Fermi level, respectively. The two states show different upward dispersions with effective electron masses of 1.1 and $1.9\,m_e$, respectively. Time-resolved 2PPE was used to measure the lifetimes of the image states *A* and *B* as 40 and 20 fs, respectively. The image states *A* and *B* are proposed to be supported by patches with monolayer and bilayer coverage, respectively. A simulation of the two states within the dielectric continuum model could not reproduce the short lifetime of the state *B*. However, a simple Kronig–Penney model for the bilayer can explain this shortcoming, and at the same time reproduce the high effective mass of the state *B*. This investigation presents the dynamics of the incomplete bilayer, which can be viewed as a laterally confined structure, and can shed some light on the role of adsorption morphology in electron dynamics.

ACKNOWLEDGMENTS

D.V. acknowledges the Max-Planck-Gesellschaft Fellowship. We thank Inge Reinhardt for careful reading of our manuscript.

[1] R. R. Cavanagh, D. S. King, J. C. Stephenson, and T. F. Heinz, J. Phys. Chem. **97**, 786 (1993).
[2] Th. Fauster and W. Steinmann, *Electromagnetic Waves: Recent Developments in Research*, edited by P. Halevi (Elsevier, Amsterdam, 1995).
[3] R. Fischer, S. Schuppler, N. Fischer, Th. Fauster, and W. Steinmann, Phys. Rev. Lett. **70**, 654 (1993).
[4] N.-H. Ge, C. M. Wong, R. L. Lingle, Jr., J. D. McNeill, K. J. Gaffney, and C. B. Harris, Science **279**, 202 (1998).
[5] R. L. Lingle, Jr., N.-H. Ge, R. E. Jordan, J. D. McNeill, and C. B. Harris, Chem. Phys. **205**, 191 (1996); D. F. Padowitz, W. R. Merry, R. E. Jordan, and C. B. Harris, Phys. Rev. Lett. **69**, 3583 (1992).
[6] J. D. McNeill, R. L. Lingle, Jr., R. E. Jordan, D. F. Padowitz, and C. B. Harris, J. Chem. Phys. **105**, 3883 (1996).
[7] L. Bartels, G. Meyer, H. Rieder, D. Velic, E. Knoesel, A. Hotzel, M. Wolf, and G. Ertl, Phys. Rev. Lett. **80**, 2004 (1998).
[8] A. Hotzel, K. Ishioka, E. Knoesel, M. Wolf, and G. Ertl, Chem. Phys. Lett. **285**, 271 (1998).
[9] M. Wolf, Surf. Sci. **377–379**, 343 (1997); M. Wolf, E. Knoesel, and T. Hertel, Phys. Rev. B **54**, R5295 (1996).
[10] E. Knoesel, A. Hotzel, and M. Wolf, J. Electron Spectrosc. Relat. Phenom. **88–91**, 577 (1998).
[11] E. Knoesel, T. Hertel, M. Wolf, and G. Ertl, Chem. Phys. Lett. **240**, 409 (1995).
[12] T. Hertel, E. Knoesel, E. Hasselbrink, M. Wolf, and G. Ertl, Surf. Sci. **317**, L1147 (1994).
[13] M. Bauer, S. Pawlik, and M. Aeschlimann, Phys. Rev. B **55**, 10040 (1997).
[14] T. Munakata, T. Sakashita, M. Tsukakoshi, and J. Nakamura, Chem. Phys. Lett. **271**, 377 (1997).
[15] T. Munakata, T. Sakashita, and K.-i. Shudo, J. Electron Spectrosc. Relat. Phenom. **88–91**, 591 (1998).
[16] T. Munakata, K. Mase, and I. Kinoshita, Surf. Sci. **286**, 73 (1993).
[17] K. Giesen, F. Hage, F. J. Himpsel, H. J. Riess, and W. Steinmann, Phys. Rev. Lett. **55**, 300 (1985).
[18] K.-H. Frank, R. Dudde, and E. E. Koch, Chem. Phys. Lett. **132**, 83 (1986).
[19] M. Xi, M. X. Yang, S. K. Jo, and B. E. Bent, J. Chem. Phys. **101**, 9122 (1994).
[20] R. Hoffmann, Rev. Mod. Phys. **60**, 601 (1988).
[21] S. J. Stranick, M. M. Kamna, and P. S. Weiss, Surf. Sci. **338**, 41 (1995).
[22] J. R. Lomas and G. Pacchioni, Surf. Sci. **365**, 297 (1996).
[23] X.-C. Guo and R. J. Madix, Surf. Sci. **341**, L1065 (1995).
[24] C. J. Craven, P. D. Hatton, C. J. Howard, and G. S. Pawley, J. Chem. Phys. **98**, 8236 (1993).
[25] X.-L. Zhou, M. E. Castro, and J. M. White, Surf. Sci. **238**, 215 (1990).
[26] P. W. Atkins, *Physical Chemistry* (W. H. Freeman, New York, 1990).
[27] A. Nilsson, N. Wassdahl, M. Weinelt, O. Karis, T. Wiell, P. Bennich, J. Hasselstrom, A. Fohlisch, J. Stohr, and M. Samant, Appl. Phys. A: Mater. Sci. Process. **65**, 147 (1997).
[28] I. Nenner and G. J. Schulz, J. Chem. Phys. **62**, 1747 (1975).
[29] T. V. W. Janssens, G. R. Castro, K. Wandelt, and J. W. Niemantsverdriet, Phys. Rev. B **49**, 14599 (1994).
[30] C. B. Harris, N.-H. Ge, R. L. Lingle, Jr., J. D. McNeill, and C. M. Wong, Annu. Rev. Phys. Chem. **48**, 711 (1997).
[31] *Handbook of Chemistry and Physics*, edited by R. C. Weast, 53rd ed. (The Chemical Rubber Co., Cleveland, 1972).
[32] P. L. de Andres, P. M. Echenique, and F. Flores, Phys. Rev. B **35**, 4529 (1987).
[33] C. Kittel, *Introduction to Solid State Physics*, 7th ed. (Wiley, New York, 1996).